Supporting Information for:

Design and Synthesis of a Family of 1D-Lanthanide-Coordination Polymers Showing Luminescence and Slow Relaxation of the Magnetization

Ana Belén Ruiz-Muelle,[a] Amalia García-García,[b] Antonio A. García-Valdivia,[b] Itziar Oyarzabal,[c] Javier Cepeda,[c] José M. Seco,[c] Enrique Colacio,[b] Antonio Rodríguez-Diéguez[b] and Ignacio Fernández[a,*]

[a] Department of Chemistry and Physics, Research Centre CIAIMBITAL, University of Almería, Ctra. Sacramento s/n, 04120 Almería, Spain. [b] Departamento de Química Inorgánica, Facultad de Ciencias, Universidad de Granada, 18071 Granada, Spain. [c] Departamento de Química Aplicada, Facultad de Química, Universidad del País Vasco (UPV/EHU), 20018 Donostia, Spain.

Contents:

S1. FT-IR (KBr) spectrum of Haapc (**1**).

S2. ^{1}H NMR spectrum of Haapc (**1**) at room temperature.

S3. ^{13}C NMR (bottom) and DEPT-135 (top) NMR spectra of Haapc (**1**) at room temperature.

S4. COSY spectrum of Haapc (**1**) at room temperature.

S5. ^{1}H,^{13}C gHMQC spectrum of Haapc (**1**) at room temperature.

S6. ^{1}H,^{13}C gHMBC spectrum of Haapc (**1**) at room temperature.

S7. FT-IR (KBr) spectrum of complex **2**.

S8. ^{1}H NMR spectrum of complex **2** at 333 K.

S9. 1D-gTOCSY spectrum of complex **2** at 333 K.

S10. ^{13}C NMR (bottom) and DEPT-135 (top) NMR spectra of complex **2** at 333 K.

S11. ^{1}H,^{13}C gHMBC spectrum of complex **2** at 333 K.

S12. Diffusion NMR Details studies of ligand Haapc (**1**) and complex **2**.

S13. Structural details of compound **8**.

S14. Continuous shape measures (CShMs)

S15. Powder X-ray Data Collection.

S16. Photoluminescence measurements.

S17. Ac susceptibility measurements.

S18. Magneto-caloric effect for gadolinium compound.

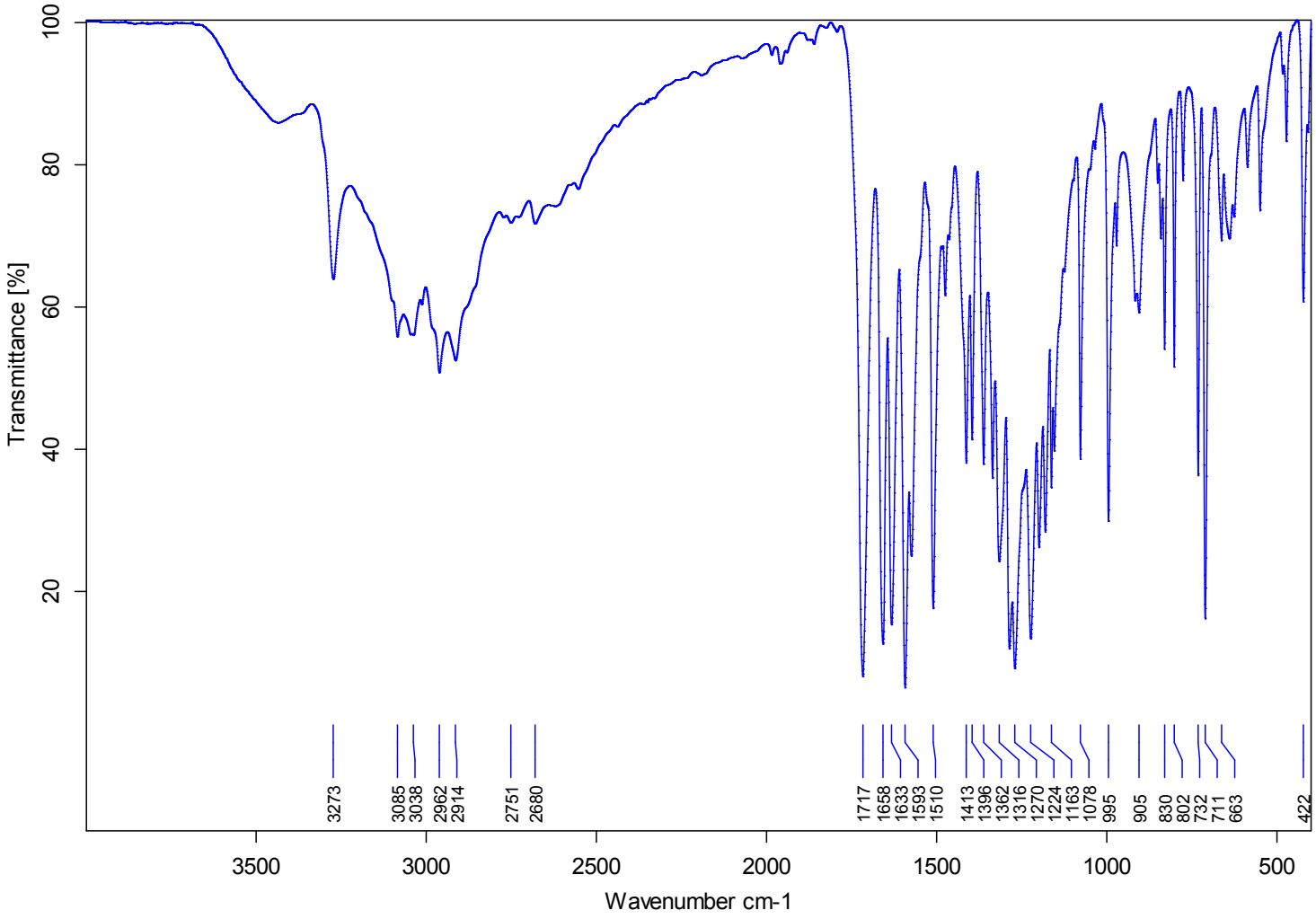

Figure S1. FT-IR (KBr) spectrum of **1**.

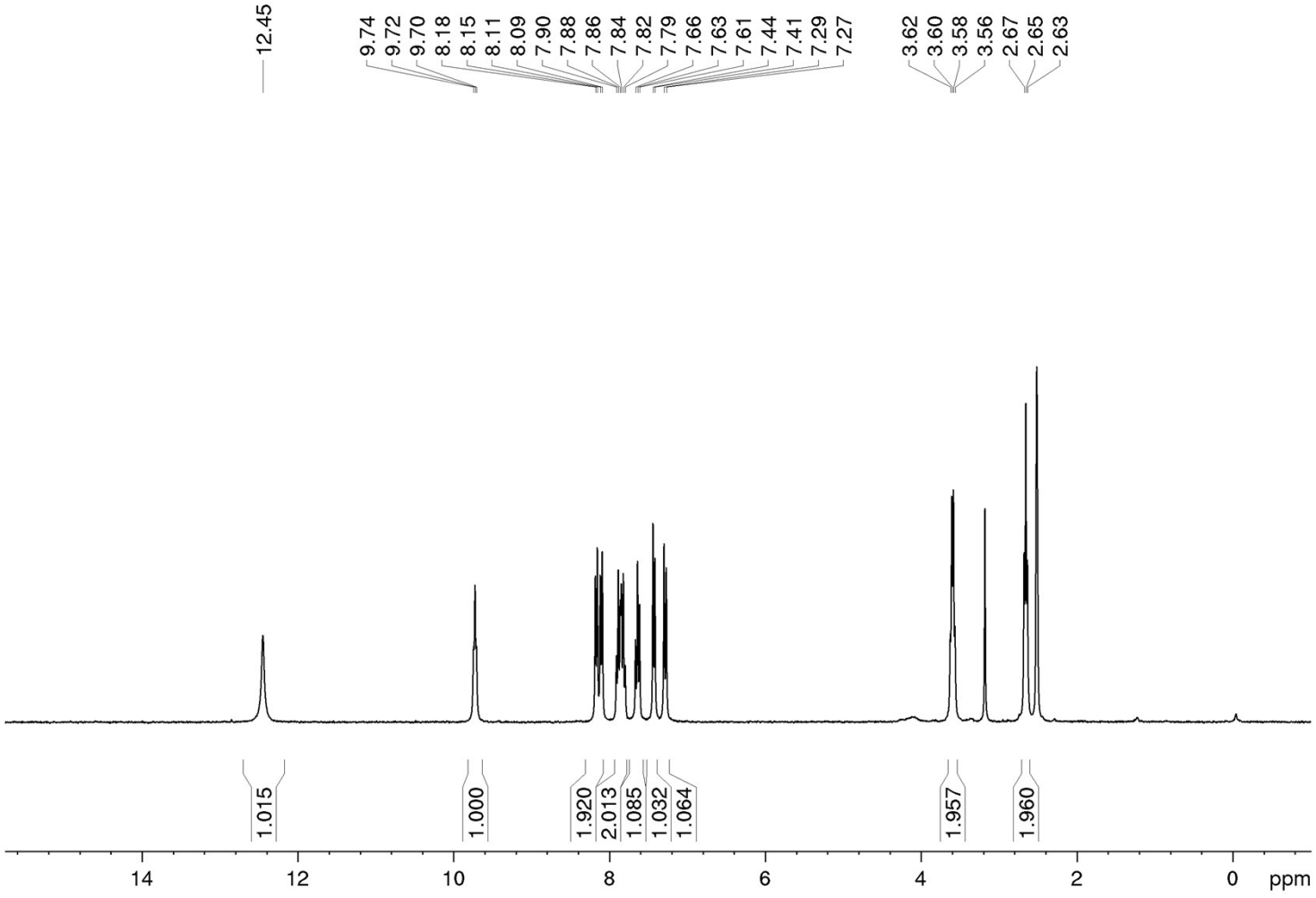

Figure S2. ^{1}H NMR spectrum of **1** in DMSO-d_6 at room temperature (300.13 MHz).

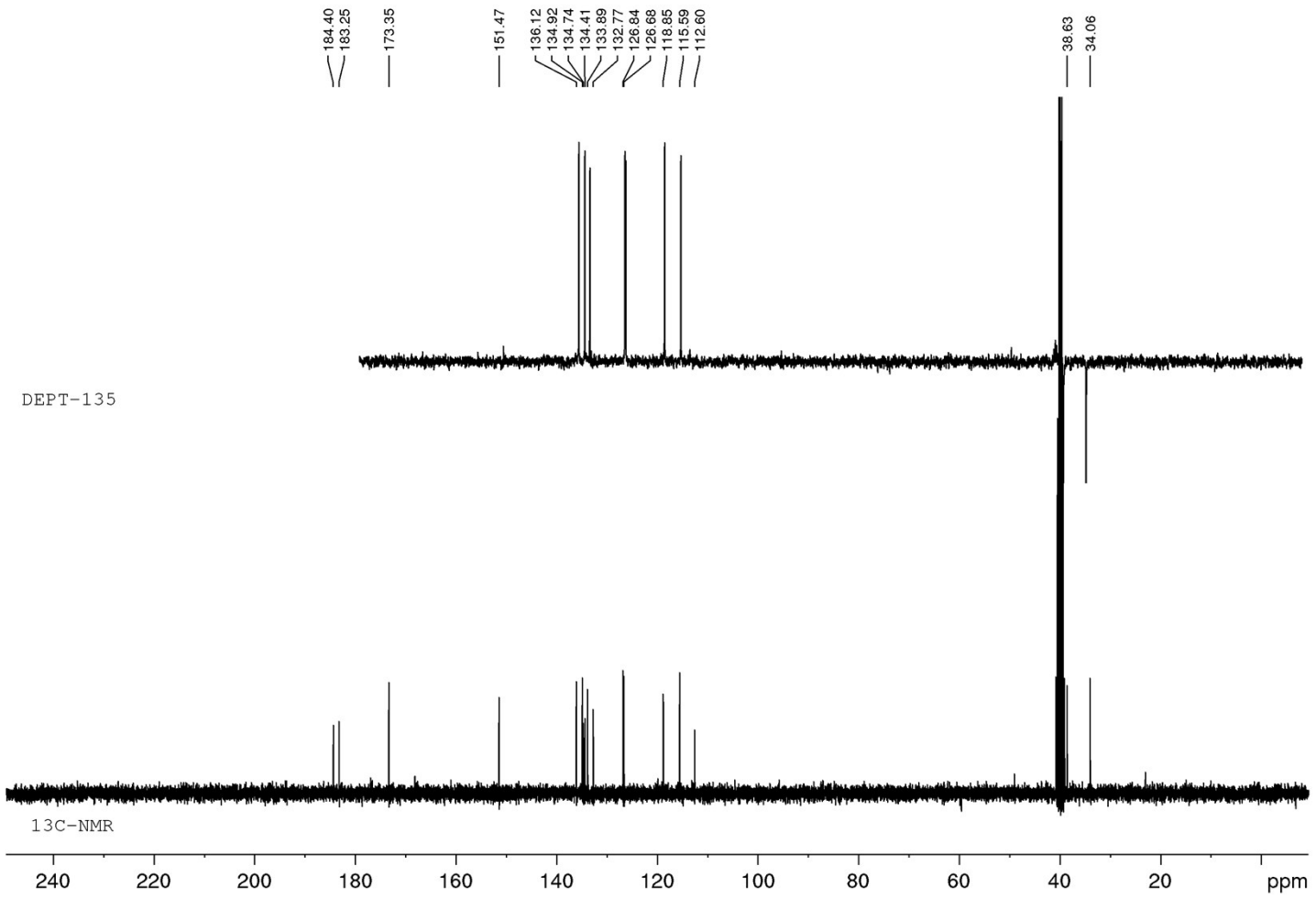

Figure S3. ^{13}C NMR (bottom) and DEPT-135 (top) NMR spectra of **1** in DMSO-d_6 at room temperature (75.47 MHz).

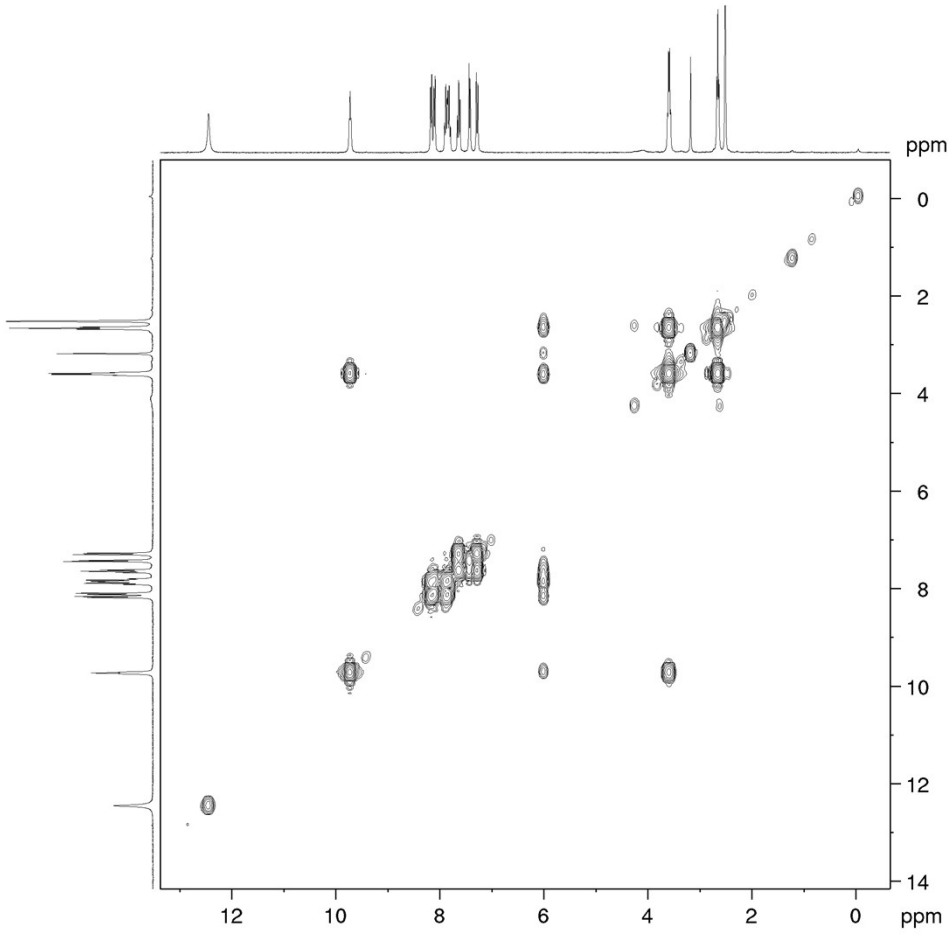

Figure S4. COSY spectrum of **1** in DMSO-d_6 at room temperature.

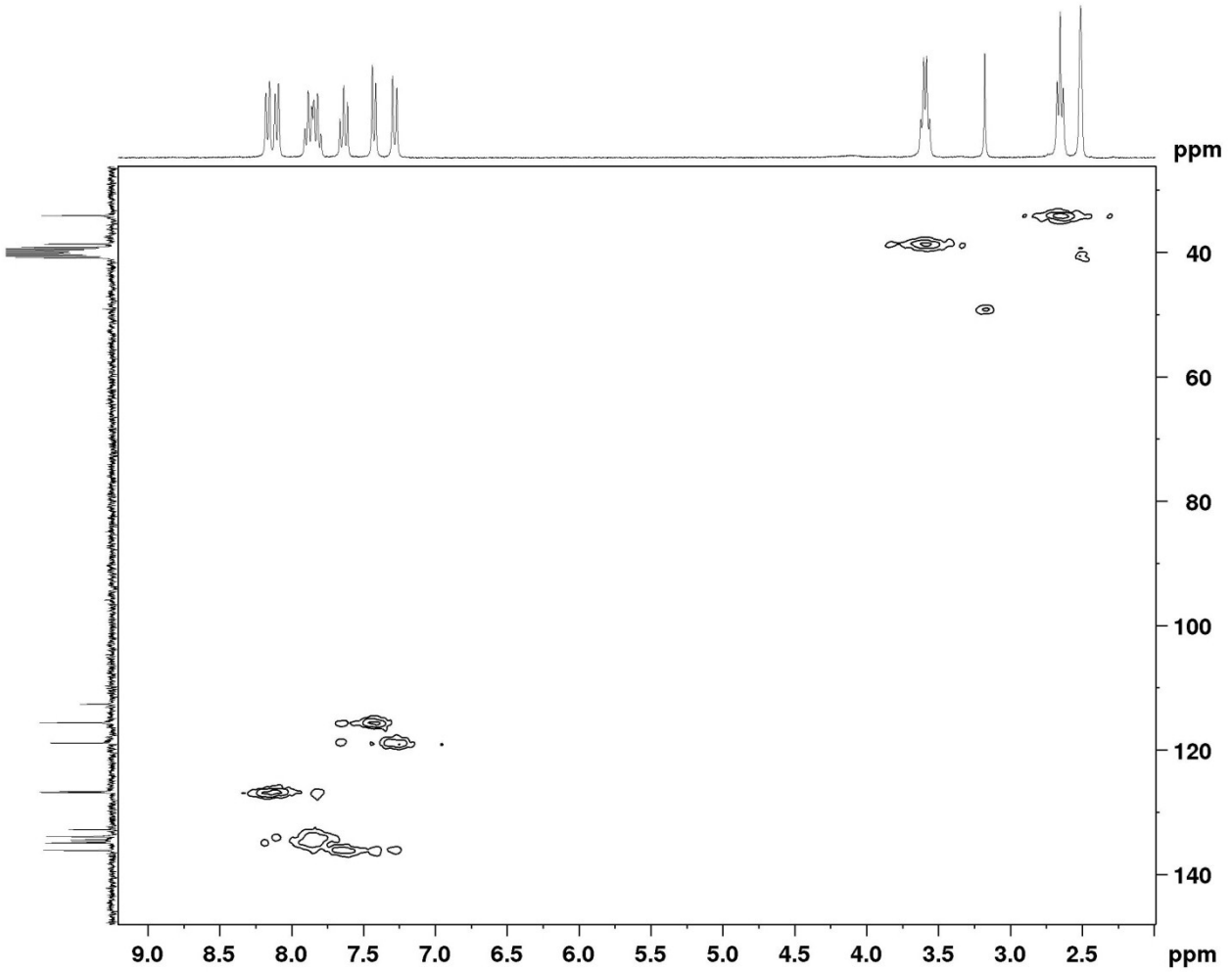

Figure S5. $^{1}H,^{13}C$ gHMQC spectrum of **1** in DMSO-d_6 at room temperature.

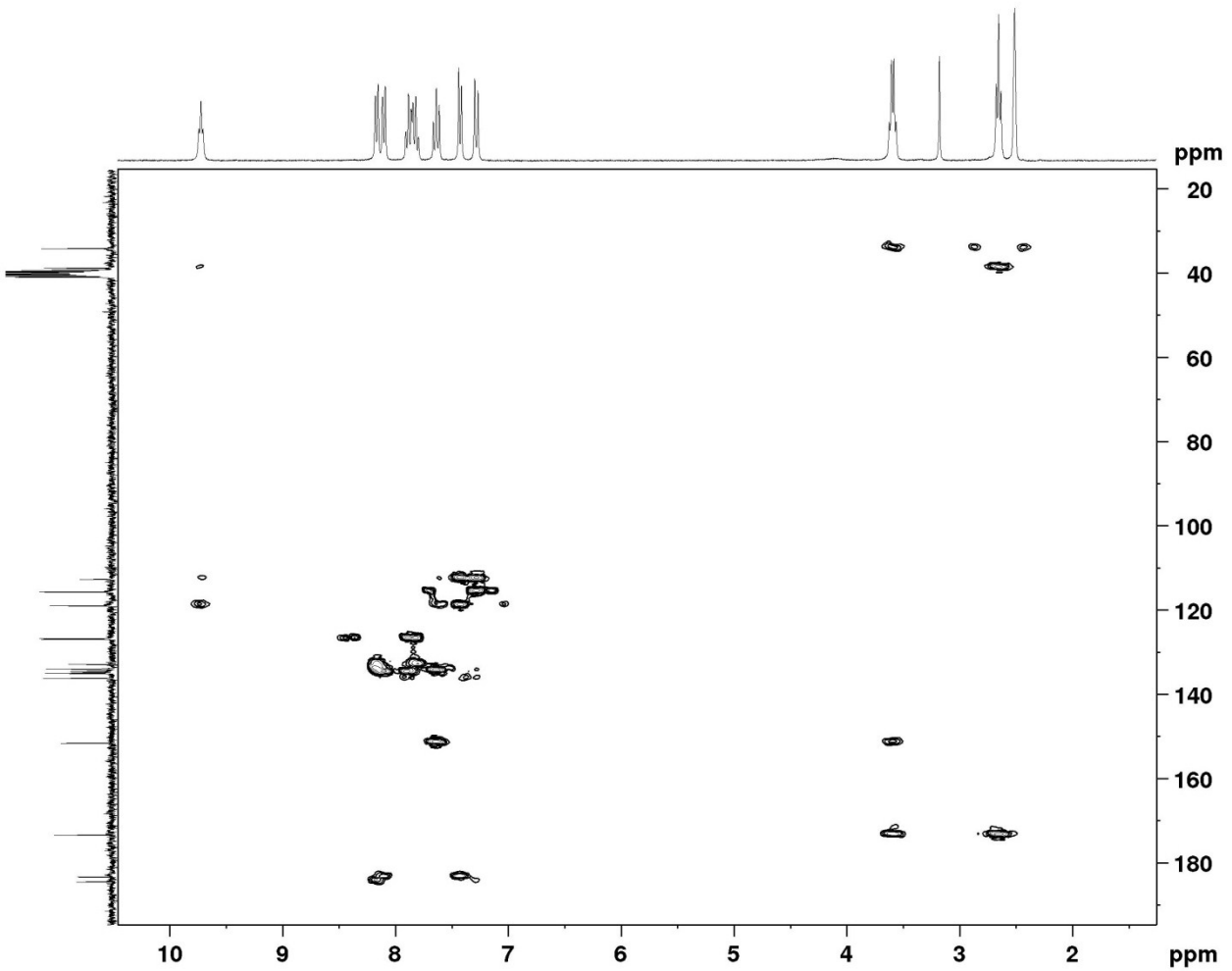

Figure S6. $^{1}H,^{13}C$ gHMBC spectrum of **1** in DMSO-d_6 at room temperature.

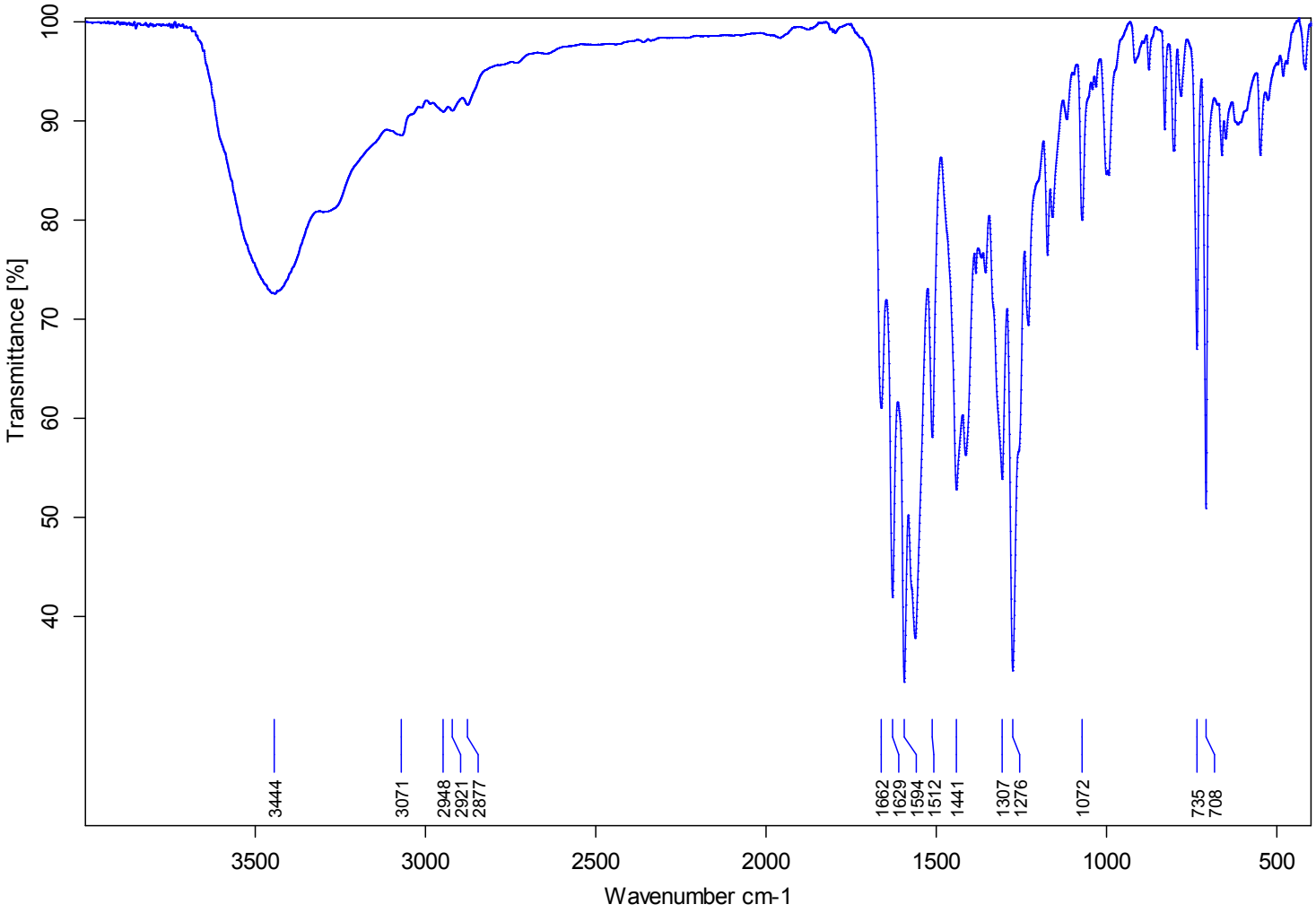

Figure S7. FT-IR (KBr) spectrum of complex **2**.

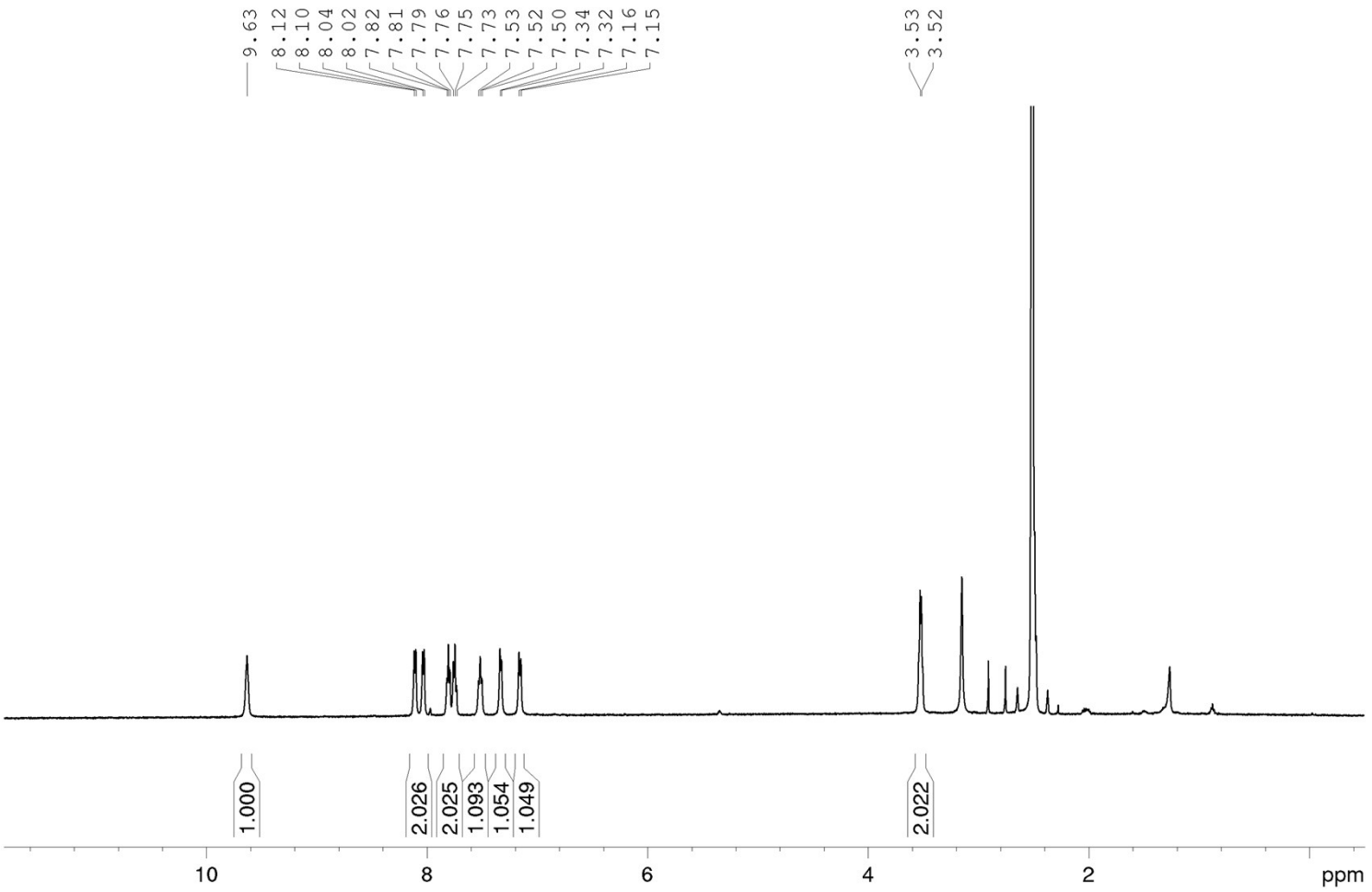

Figure S8. ^{1}H NMR spectrum of complex **2** in DMSO-d_6 at 333 K (500.13 MHz).

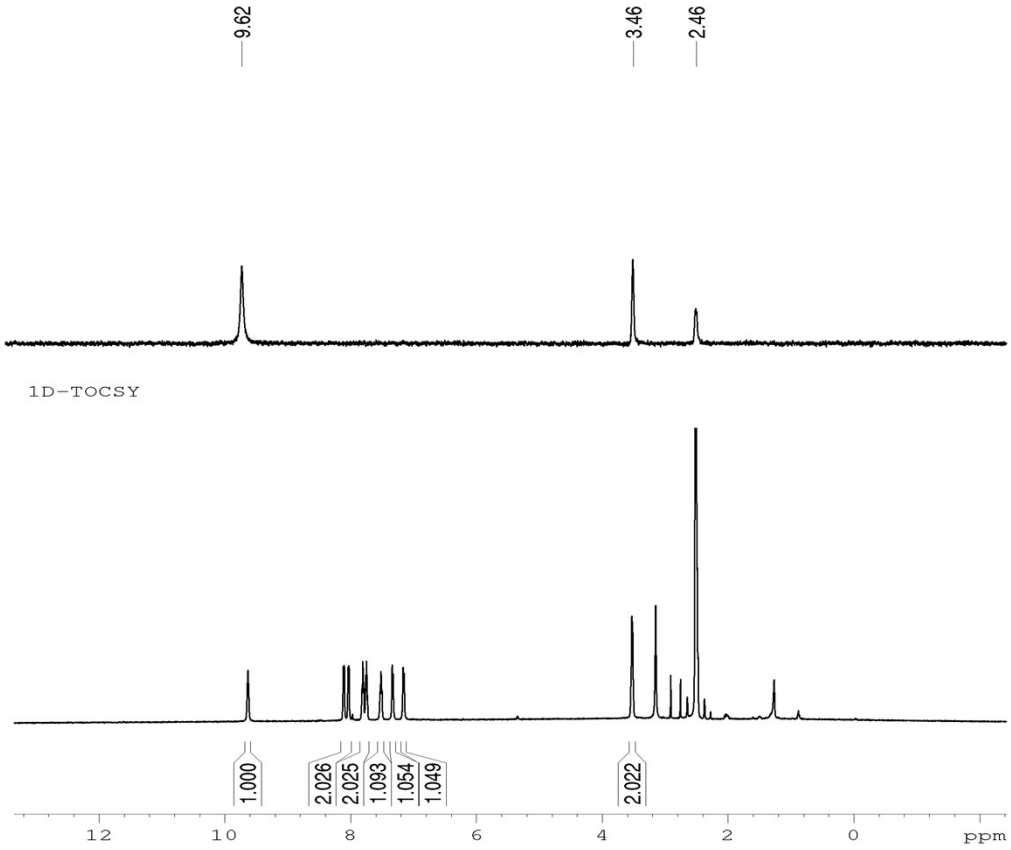

Figure S9. 1D-gTOCSY spectrum of complex **2** in DMSO-d_6 at 333 K.

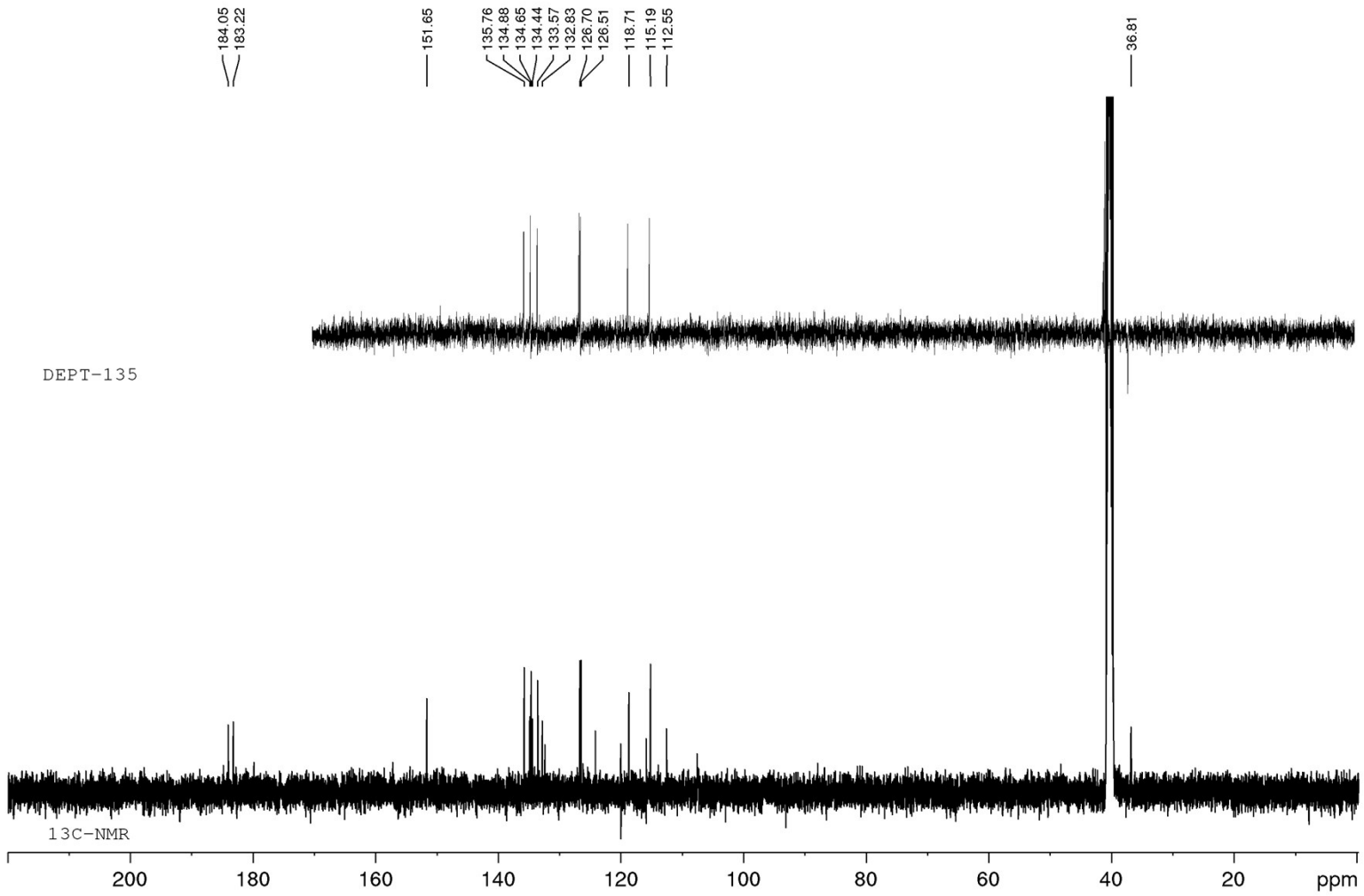

Figure S10. ^{13}C NMR (bottom) and DEPT-135 (top) NMR spectra of complex **2** in DMSO-d_6 at 333 K (126 MHz).

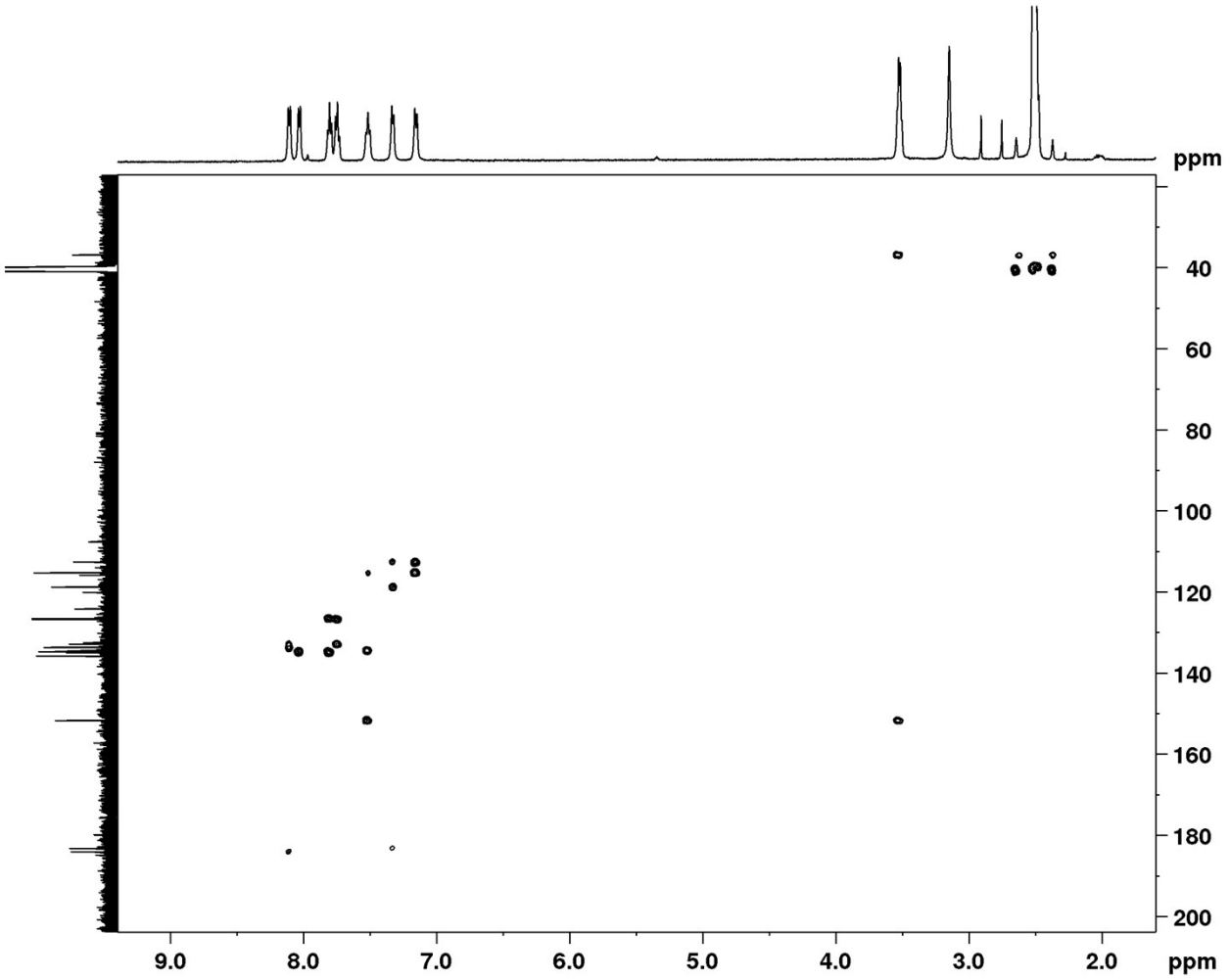

Figure S11. $^{1}H,^{13}C$ gHMBC spectrum of complex **2** in DMSO-d_6 at 333 K.

S12. Diffusion NMR Details studies.

PGSE NMR diffusion measurements were carried out using the stimulated echo sequence and monopolar pairs pulses (stegp).[1] A sine shape was used for the gradient pulses and their strength varied automatically in the course of the experiments. The *D* values were determined from the slope of the regression line $\ln(I/I_0)$ versus G^2, according to the following equation, and employing the DiffAtOnce package.[2] I/I_0 = observed spin echo intensity/intensity without gradients, G = gradient strength, Δ = delay between the midpoints of the gradients, D = diffusion coefficient, δ = gradient length.

$$Ln(\frac{I}{I_0}) = -(\gamma\delta)^2(\Delta - \frac{\delta}{4})D\frac{4}{\pi^2}G^2$$

The measurements were carried out without spinning. Gradient calibration was carried out by means of a diffusion measurement of HDO in D_2O (D(HDO) = 1.902 10^{-9} m^2 s^{-1}).[3] To check reproducibility, three different measurements with different diffusion parameters (δ and/or Δ) were always carried out. The experimental error in *D* values was estimated to be smaller than ±2%. All of the data leading to the reported *D* values afforded lines whose correlation coefficients were above 0.999 and 8 to 12 points were used for regression analysis. To check reproducibility, three different measurements with different diffusion parameters (δ and/or Δ) were always carried out. The gradient strength was incremented in 4–8% steps from 2–10% to 98% so that, depending on signal: noise, 12–25 points could be used for regression analysis. The recovery delay was set to 5 times T_1. All diffusion processing and molecular size estimation were performed by using the DiffAtOnce software package available at www.diffatonce.com.

S13. Structural details of compound 8.

Table S1. Structural parameters (Å, º) of π–π interactions of compound **8**.[a]

Ring...Ring[b]	α	DC	β	DZ	Dist.
1A–1A(v)	0.02	3.582(3)	21.94	3.32	3.17–3.56

[a] Symmetry: (v) –y – 1, –x + 2, –z + 1/2; (vi) –y + 3/2, x + 3/2, z + 3/4. α: dihedral angle between mean planes of the rings (°), DC: distance between ring centroids (Å), β: angle between DC vector and normal to plane(I) (°), DZ: perpendicular distance of the centroids of ring(I) on plane of ring(II) (Å), Dist.: shorter distances between non-hydrogen atoms of rings (I) and (II). [b] Ring: **1A**: C1A, C2A, C7A, C8A, C9A, C14A.

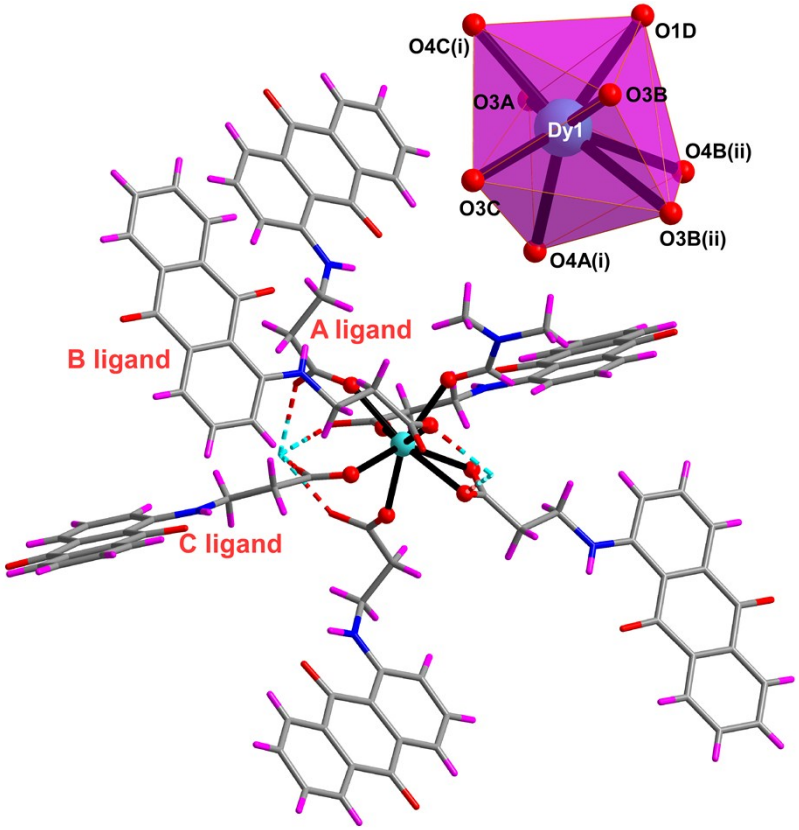

Figure S12. Excerpt of the compound **8** showing the two successive dimeric entities of the 1D chain as well as the coordination sphere.

S14. Continuous shape measures (CShMs)

Table S2. Continuous Shape Measurements for Compound **8**.

OP-8	D8h	Octagon
HPY-8	C7v	Heptagonal pyramid
HBPY-8	D6h	Hexagonal bipyramid
CU-8	Oh	Cube
SAPR-8	D4d	Square antiprism
TDD-8	D2d	Triangular dodecahedron
JGBF-8	D2d	Johnson gyrobifastigium J26
JETBPY-8	D3h	Johnson elongated triangular bipyramid J14
JBTPR-8	C2v	Biaugmented trigonal prism J50
BTPR-8	C2v	Biaugmented trigonal prism
JSD-8	D2d	Snub diphenoid J84
TT-8	Td	Triakis tetrahedron
ETBPY-8	D3h	Elongated trigonal bipyramid

OP-8	HPY-8	HBPY-8	CU-8	**SAPR-8**	TDD-8	JGBF-8
32.048	21.324	13.305	7.972	**1.642**	2.261	14.384

JETBPY-	JBTPR-8	BTPR-8	JSD-8	TT-8	ETBPY-
26.907	2.917	1.994	5.428	8.799	22.259

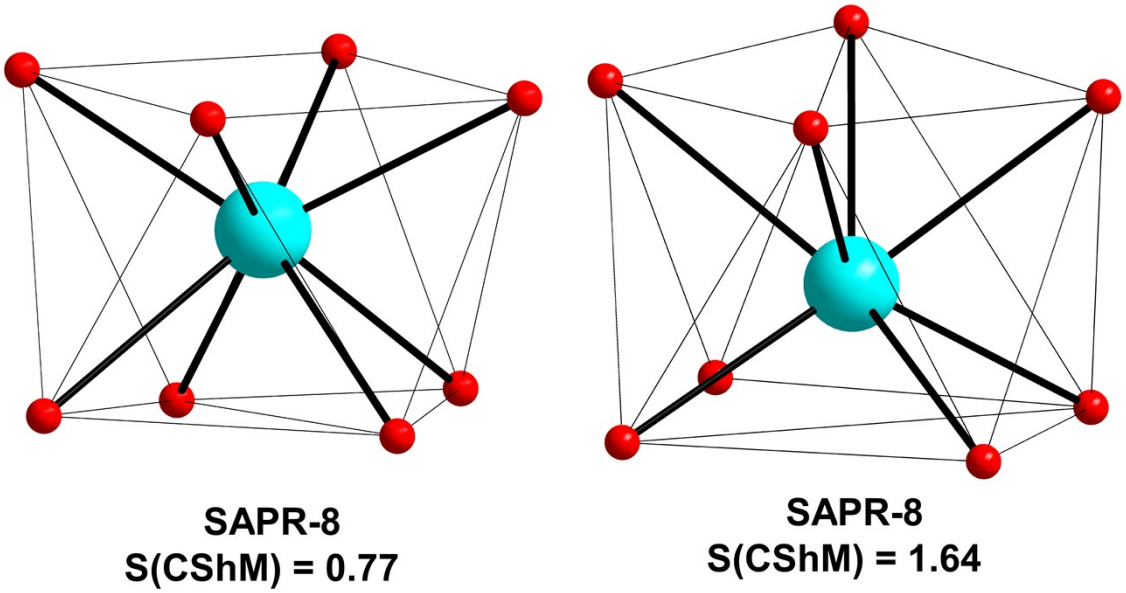

Figure S13. DyO_8 coordination environments for compound **8** and $\{[Dy((NH_2)_2\text{-}bdc)_{1.5}(DMF)_2]\cdot DMF\cdot H_2O\}_n$[4] with their continuous shape measures.

S15. Powder X-ray Data Collection.

Table S3, S4 and Figure S13 summarize the data resulting from the PXRD pattern-matching analyses performed on compounds **2–9**, which confirm the isostructural nature and purity of all samples.

Table S3. PXRD pattern-matching results of compounds **2–5**.

	2	**3**	**4**	**5**
Empirical formula	$C_{54}H_{43}N_4O_{13}Y$	$C_{54}H_{43}LaN_4O_{13}$	$C_{54}H_{43}NdN_4O_{13}$	$C_{54}H_{43}EuN_4O_{13}$
Formula weight	1044.84	1094.84	1100.18	1107.90
Crystal system	triclinic	triclinic	triclinic	triclinic
Space group	*P–1*	*P–1*	*P–1*	*P–1*
a (Å)	8.1575(4)	8.154(2)	8.154(2)	8.154(2)
b (Å)	17.4805(8)	8.154(2)	8.154(2)	8.154(2)
c (Å)	17.9640(6)	20.052(4)	20.052(4)	20.052(4)
α (°)	62.669(2)			
β (°)	80.922(3)			
γ (°)	88.786(2)			
V (Å^3)	1260.7(7)	1333.3(6)	1333.3(6)	1333.3(6)
Z	2	4	4	4
Chi^2	1.94	2.94	2.94	2.94

Table S4. PXRD pattern-matching results of compounds **6–9.**

	6	**7**	**8**	**9**
Empirical formula	$C_{54}H_{43}GdN_4O_{13}$	$C_{54}H_{43}N_4O_{13}Tb$	$C_{54}H_{43}DyN_4O_{13}$	$C_{54}H_{43}ErN_4O_{13}$
Formula weight	1113.19	1114.86	1118.44	1123.20
Crystal system	triclinic	triclinic	triclinic	triclinic
Space group	*P–1*	*P–1*	*P–1*	*P–1*
a (Å)	8.1575(4)	8.154(2)	8.154(2)	8.154(2)
b (Å)	17.4805(8)	8.154(2)	8.154(2)	8.154(2)
c (Å)	17.9640(6)	20.052(4)	20.052(4)	20.052(4)
α (°)	62.669(2)			
β (°)	80.922(3)			
γ (°)	88.786(2)			
V (Å^3)	1260.7(7)	1333.3(6)	1333.3(6)	1333.3(6)
Z	2	4	4	4
Chi^2	1.94	2.94	2.94	2.94

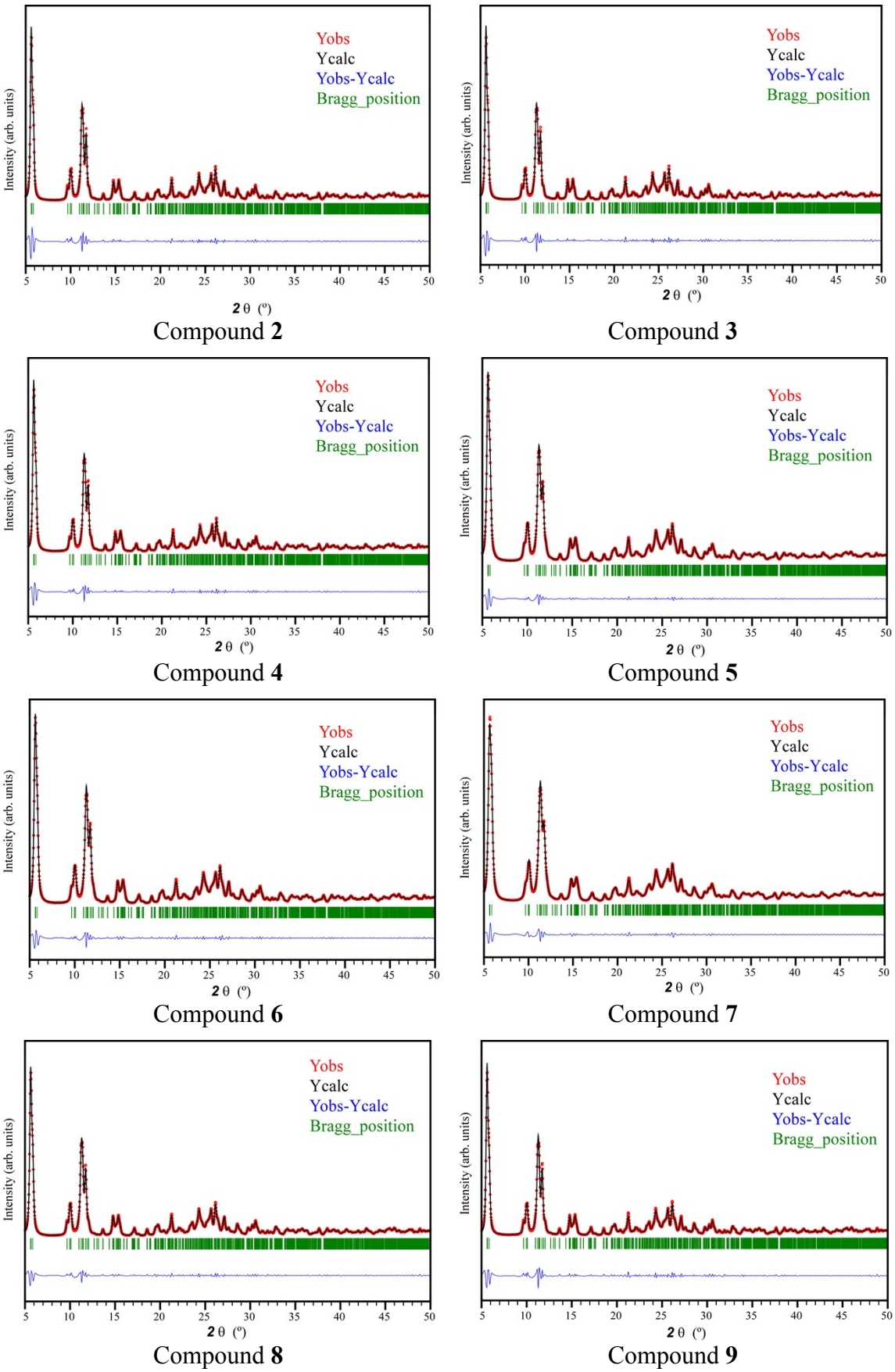

Figure S14. Comparison of experimental difractogram and the theoretical one with their full profile pattern-matching analyses.

S16. Photoluminescence measurements.

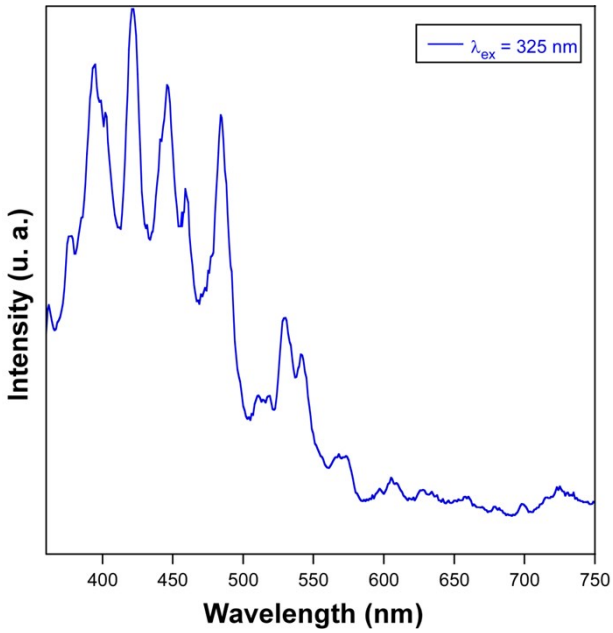

Figure S15. Room temperature emission spectra of compound **6** under excitation at 325 nm.

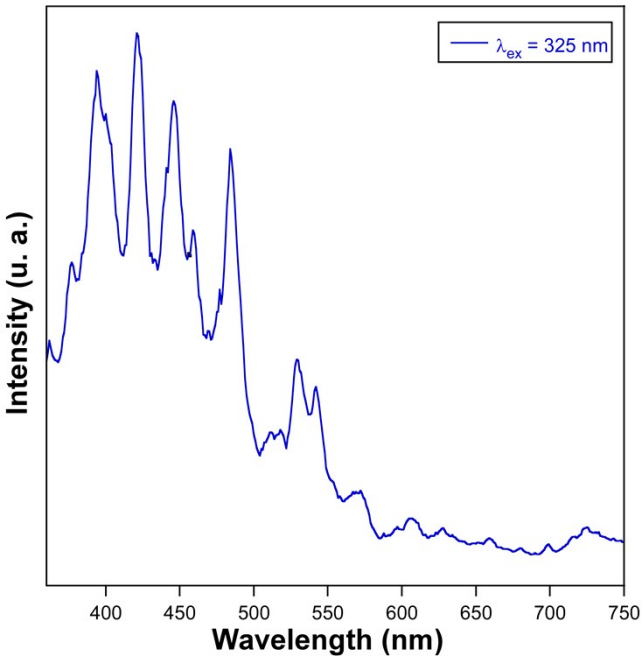

Figure S16. Room temperature emission spectra of compound **5** under excitation at 325 nm.

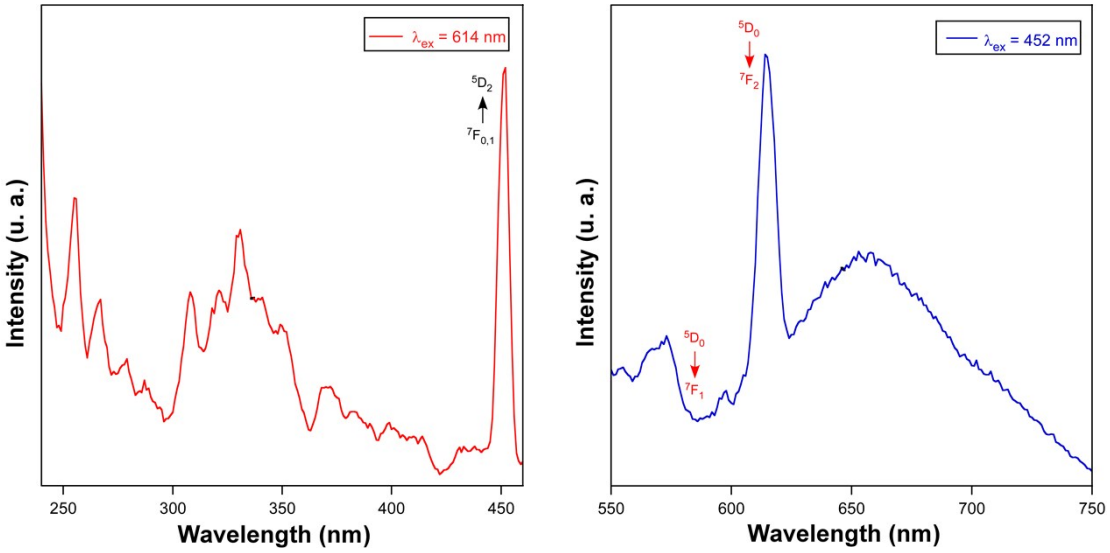

(a)

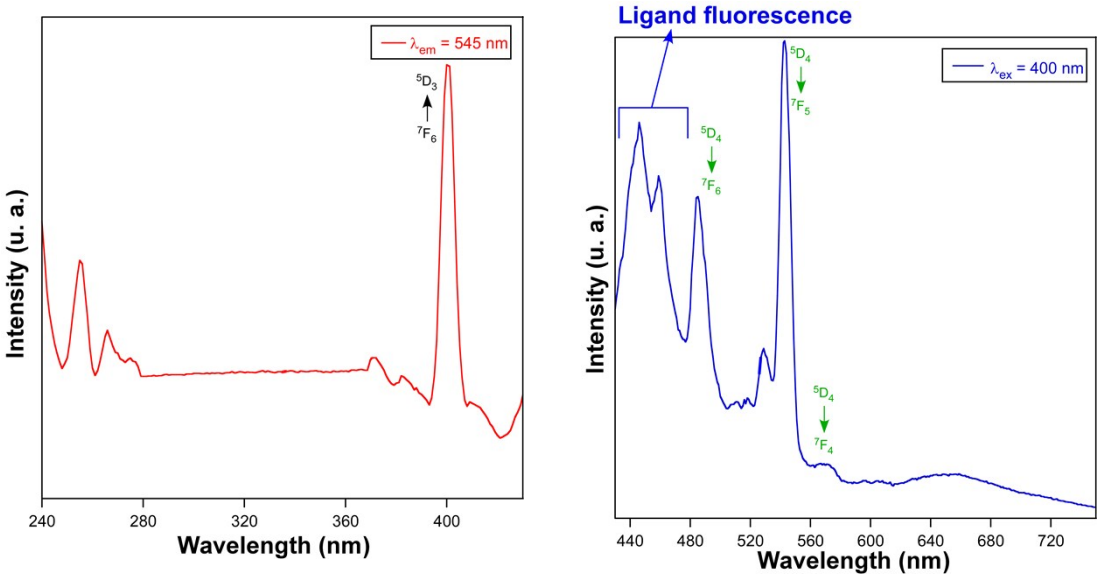

(b)

Figure S17. Room temperature excitation (red line) and emission (blue line) spectra of compounds **(a) 5** and **(b) 7**.

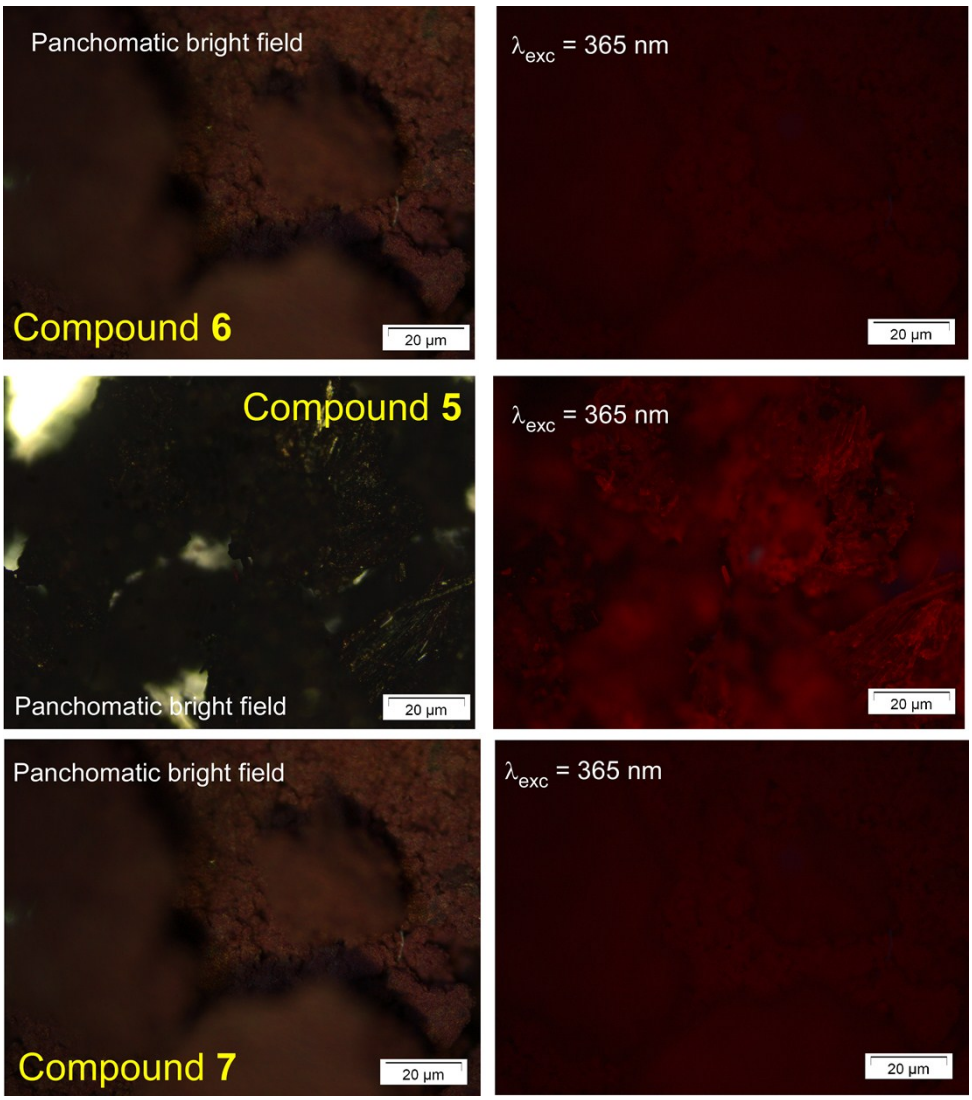

Figure S18. Micro-PL images taken on crystals or polycrystalline samples of compounds **5**–**7** under panchromatic field and UV irradiation (λ_{exc} = 365 nm).

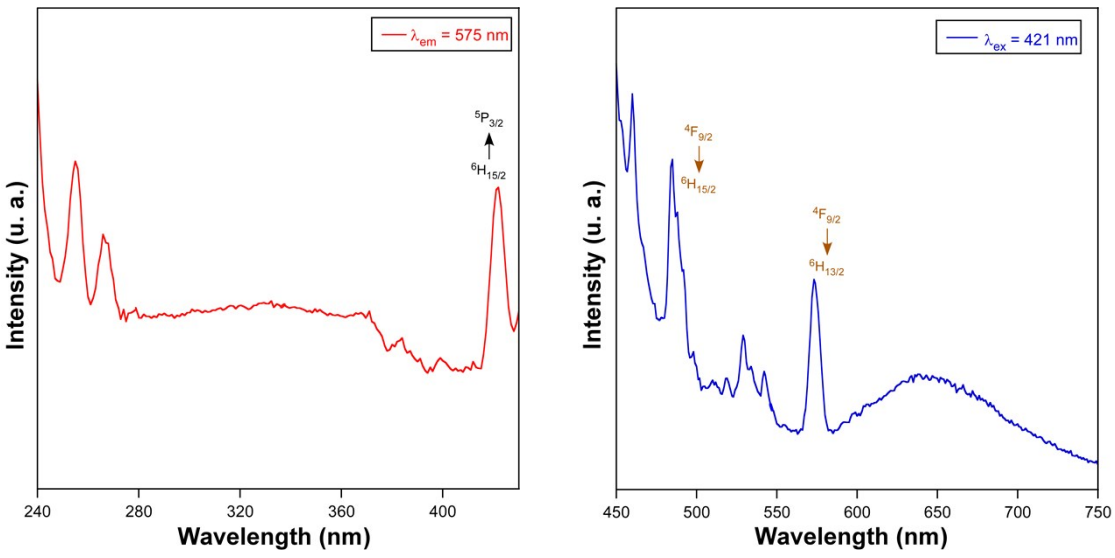

Figure S19. Room temperature excitation (red) and emission (blue) spectra of compound **8**.

S17. Ac susceptibility measurements.

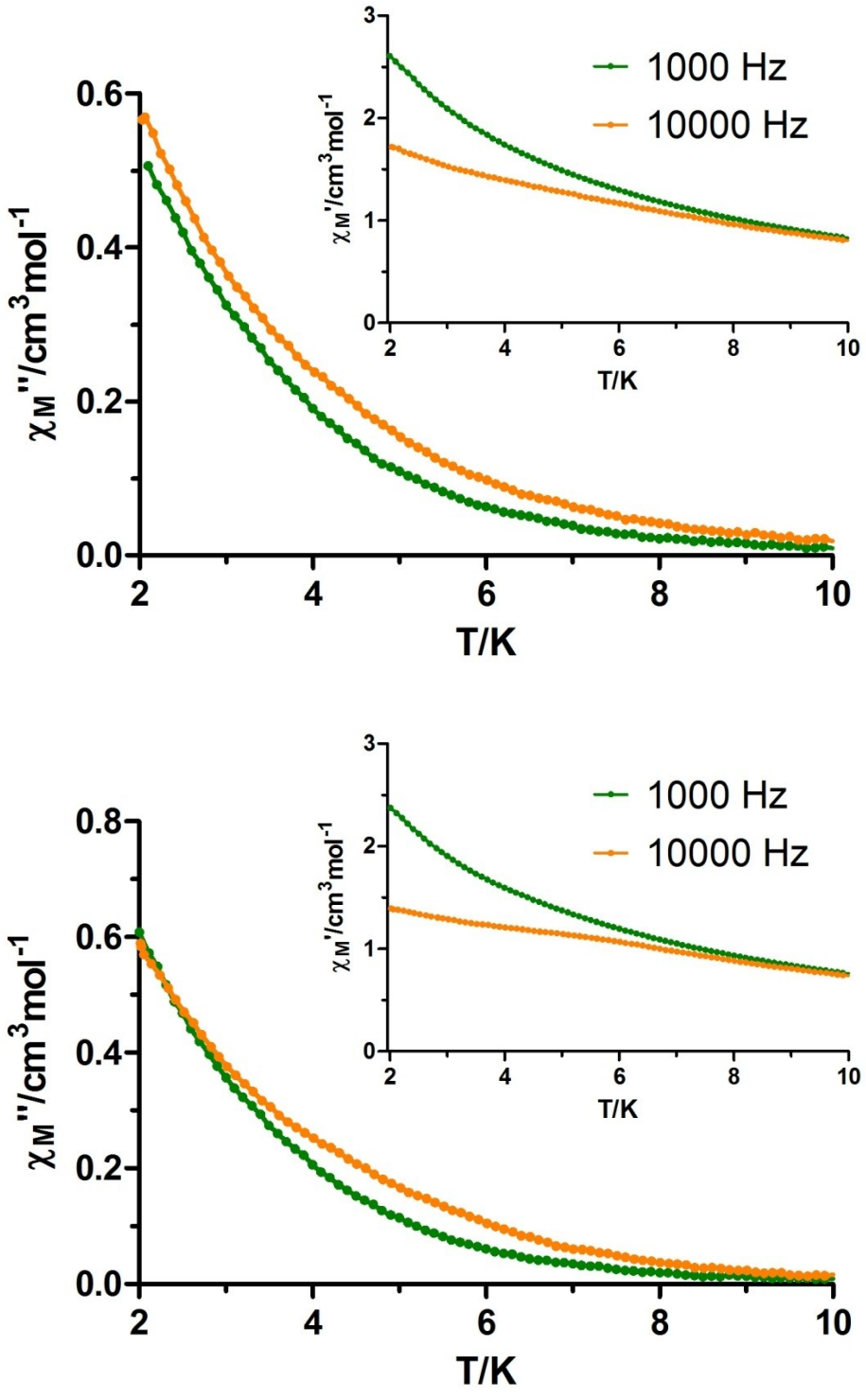

Figure S20. Temperature dependence of out-of-phase components of the *ac* susceptibility under 1000 Oe *dc* field for the diluted complexes (Dy:Y of 1:3) (top) and (Dy:Y of 1:6) (bottom). Inset: temperature dependence of in-phase components of the *ac* susceptibility under 1000 Oe *dc* field for the diluted complexes (Dy:Y of 1:3) (top) and (Dy:Y of 1:6) (bottom).

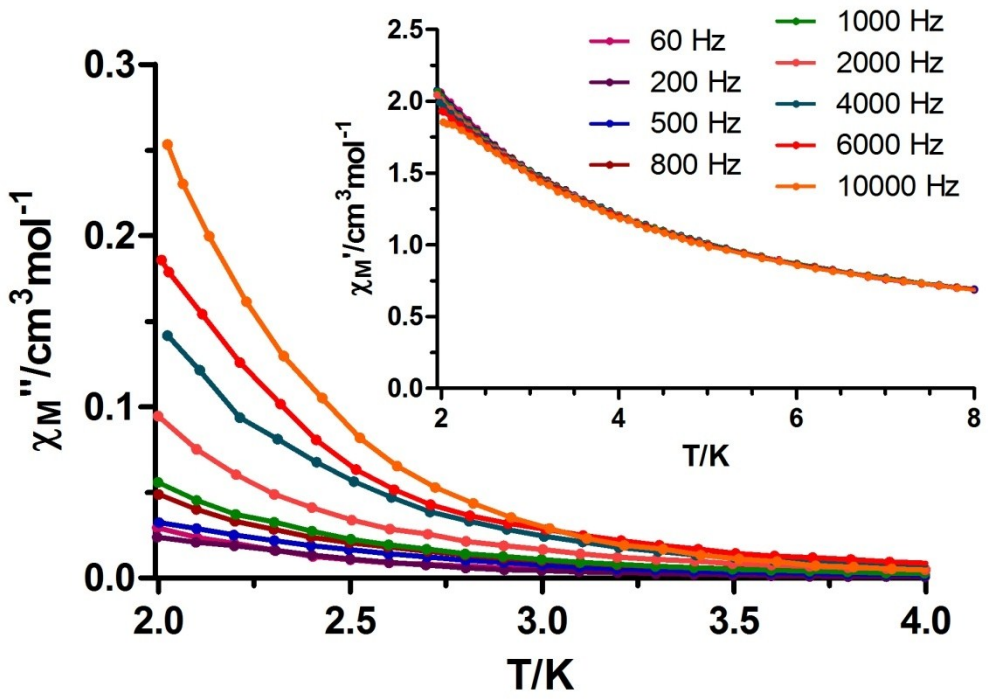

Figure S21. Temperature dependence of in-phase (inset) and out-of-phase components of the *ac* susceptibility under 1000 Oe *dc* field for the Er(III) complex.

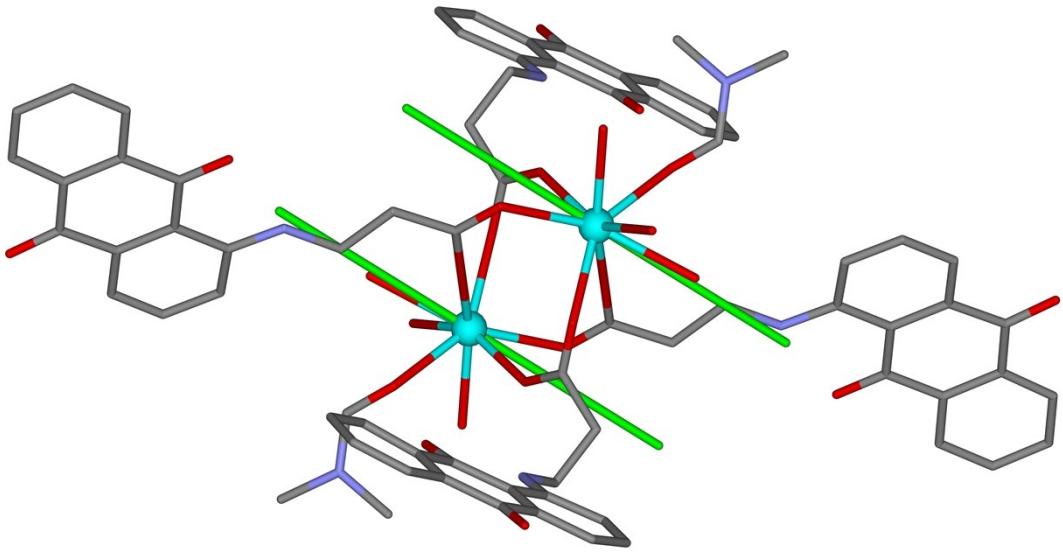

Figure S22. Orientation of the magnetic moment (Green line) for compound **8**.

S18. Magneto-caloric effect for gadolinium compound.

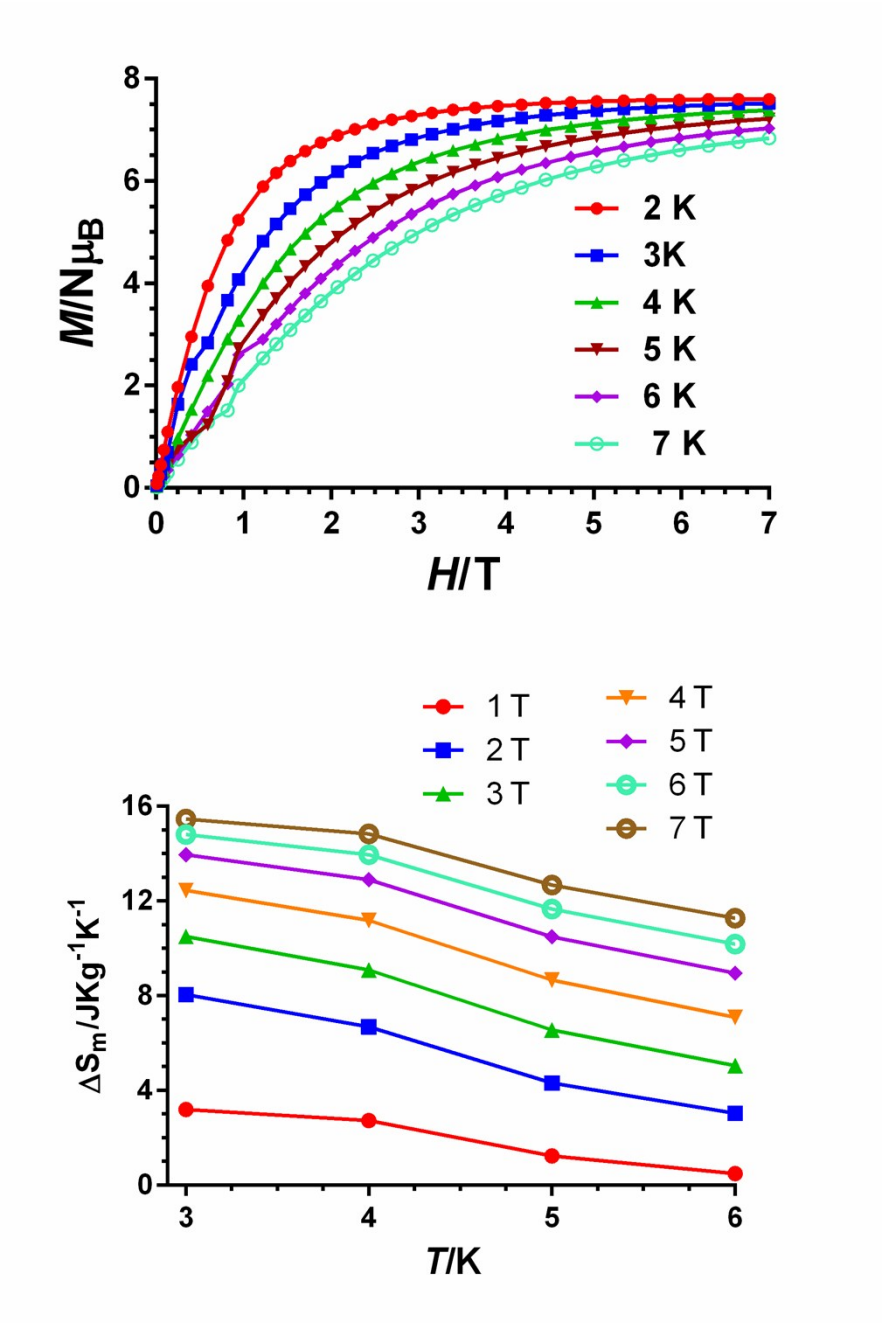

Figure S23.- (Top) The field dependence of the magnetization plots for **1** between 2 and 7 K and (bottom) magnetic entropy changes ($-\Delta S_m$) calculated from the experimental magnetization data from 1 to 7 T and temperatures from 3 to 6 K (points). Solid lines are only a guide for the eye.

REFERENCES

1 D. H. Wu; A. D. Chen; C. S. Johnson, *J. Magn. Reson. Ser., A* **1995**, *115*, 260.

2 DiffAtOnce® is a registered program developed by I. Fernández and F. M. Arrabal-Campos in the University of Almería (Spain). 2013.

3 H. J. V. Tyrrell; K. R. Harris, *Diffusion in Liquids*, Butterworths, London, 1984.

4 I. Oyarzabal, B. Fernández, J. Cepeda, S. Gómez-Ruiz, A. J. Calahorro, J. M. Seco, A. Rodríguez-Diéguez, *CrystEngComm*, 2016, **18**, 3055.